Artificial Intelligence and Emerging Technologies
https://www.sciltp.com/journals/aiet

Article

Hybrid Health Indicator Based Fusion Ahead Degradation Prediction for Proton Exchange Membrane Fuel Cell

Haolong Li [1,2], Shuiying Yu [3], Shichuan Wang [1,*], Dongqi Zhao [2], Liyan Zhang [2] and Qihong Chen [2]

[1] School of Traffic Transportation of Engineering, Wuhan Institute of Shipbuilding Technology, Wuhan 430050, China
[2] School of Automation, Wuhan University of Technology, Wuhan 430070, China
[3] Faculty of Computer and Information Technology, Wuhan Institute of Shipbuilding Technology, Wuhan 430050, China
* Correspondence: shichuan1995@qq.com

How To Cite: Li, H.; Yu, S.; Wang, S.; et al. Hybrid Health Indicator Based Fusion Ahead Degradation Prediction for Proton Exchange Membrane Fuel Cell. *Artificial Intelligence and Emerging Technologies* **2026**, *3*(3), 11. https://doi.org/10.53941/aiet.2026.100011

Received: 14 April 2026
Revised: 22 May 2026
Accepted: 14 July 2026
Published: 7 September 2026

Abstract: The decay state is the key indicator to reflect the health of a proton exchange membrane fuel cell (PEMFC). The existing static health indicators (HIs) fail to precisely represent the dynamic degradation of the PEMFC, resulting in low long-term forecasting precision of the data-driven methods. A hybrid HI and fusion ahead prediction method is proposed in this paper to achieve precise long-term decay prediction of PEMFC with limited data. Firstly, the RC-RLQ equivalent circuit equation is proposed to extract the polarization resistance from the electrochemical impedance spectroscopy data and form a hybrid HI with the voltage to accurately reflect the degradation behavior of the PEMFC under full operating conditions. Secondly, Empirical Mode Decomposition decomposes the hybrid HI into multiple Intrinsic Mode Functions to increase the inputs for Bidirectional Long Short-Term Memory (BiLSTM) in data-limited situations. Third, the sparrow search algorithm is employed to automatically optimize the optimal parameters of BiLSTM, which reduces the complexity of the prediction model and improves the model generalizability. Finally, a fusion ahead prediction method with hybrid HI is used to realize 10-step ahead decay prediction with limited data. The forecasting performance of the fusion ahead prediction algorithm is verified with real PEMFC data. With 185 h of training data, the 10-step RUL prediction error of the fusion ahead prediction method is only 0.63%. The results of the degradation prediction prove that the fusion ahead prediction method can precisely represent long-term degradation behavior of PEMFC, which is significant for the routine maintenance and control of PEMFC.

Keywords: proton exchange membrane fuel cell; multi-step ahead prediction; remaining useful life; hyperparameter optimization; health indicator

1. Introduction

Proton exchange membrane fuel cell (PEMFC) are highly regarded for their potential as for clean and non-polluting and high energy conversion efficiency [1–3]. The limited lifetime of PEMFCs is a key constraint to their widespread commercial application [4,5]. The key role of decay prediction is to evaluate the remaining useful life (RUL) of the PEMFC according to its decay trend and to take health measures before failure occurs [6,7]. The research on PEMFC degradation prediction can inform the scientific basis of health maintenance for fuel cell systems. Users can adjust the health management strategy in time based on the change of the degradation trend to improve the performance and RUL of the PEMFC [8].

Various operation influencing factors of PEMFC restrict the accuracy of long-term decay prediction in PEMFC [9]. Therefore, it is crucial to find efficacious methods that can improve the precision of PEMFC degradation forecasts. The mainstream prediction methods for PEMFC decay can be categorized into the following three types: model-based algorithms [10,11], data-based algorithms [12,13], and hybrid algorithms [14,15]. The electrochemical reactions within the PEMFC are very complex, and there is currently no unified modeling approach that can comprehensively and accurately characterize its degradation process. The shortcoming of model-based prediction methods is the difficulty of modeling the PEMFC mechanism with high precision with existing methods. Hybrid algorithms combine model-based and data-driven methods. Essentially, the hybrid algorithms are based on the fusion of modeling and data methods, which makes them difficult to model and complex to solve.

Compared to model-based algorithms and hybrid algorithms, the data-driven algorithms require no understanding of the internal mechanics of PEMFC, which has the advantage of a small computational burden and is simple to deploy [16]. A bidirectional long short-term memory (BiLSTM) model base on decay mechanism is used to forecast decay of the PEMFC stack in [17]. However, the training data proportion of this method is 50% of the real data, which is unable to provide reliable decay predictions in the early operational of the PEMFC. A time series combination model based on LSTM is proposed in [18], which has high forecast accuracy after training with 50% voltage data. But this method is poor at predicting decay of dynamic operating conditions. The output voltage has volatility and randomness, and its usage as health indicator (HI) tends to cause the prediction method to accumulate errors in the iterations. The prediction methods in the above research use voltage as HI, which cannot realize accurate long-term prediction with limited data.

The prediction methods discussed above mainly use voltage as the health indicator (HI), which limits their ability to achieve accurate long-term prediction under limited data conditions. In fact, PEMFC operating parameters also contain degradation-related information. Therefore, many studies have incorporated operating parameters into prediction models to improve degradation prediction accuracy. In [19], the reactant pressure and temperature of PEMFCs are used as HIs, and the multi-feature input capability of the echo state network (ESN) is exploited to enhance forecasting performance. However, operating parameters alone cannot fully characterize PEMFC degradation, since the aging process is also affected by internal electrochemical states and other coupled factors. To further enrich degradation information, a hybrid method combining extreme learning machine and fuzzy extension broad learning system is proposed in [20], where 13 PEMFC operating parameters are used as input HIs for degradation prediction. Although multiple operating features can provide more information, they also increase the computational complexity of the prediction model. Under limited data conditions, excessive input features may lead to overfitting and reduce the generalization ability of the model. Therefore, relying only on PEMFC operating parameters as HIs may be insufficient for robust long-term degradation prediction. The IEEE PHM 2014 Data Challenge is also used as a prognostic benchmark [21].

Overall, accurate PEMFC degradation prediction with limited data still faces the following challenges:

(1) Voltage and operating parameters are easily affected by load-current variations and operating-condition fluctuations. As static HIs, they cannot accurately distinguish intrinsic degradation behavior from non-degradation disturbances.
(2) PEMFC aging data usually exhibit non-stationary trends and strong fluctuations, which weakens the prediction accuracy and adaptability of existing methods under limited data conditions.
(3) Multi-feature prediction models tend to suffer from high computational complexity and overfitting when training data are insufficient, resulting in poor generalization performance.

To address the above challenges, this paper proposes a fusion prediction method with a hybrid health indicator (HI) for accurate long-term remaining useful life (RUL) prediction under limited data conditions. First, an RC-RLQ equivalent circuit model is developed to extract the polarization resistance from electrochemical impedance spectroscopy (EIS) data. Then, a hybrid HI integrating polarization resistance and voltage is constructed to characterize the degradation behavior of PEMFCs under full operating conditions. Furthermore, a fusion ahead prediction method (FAPM), which combines empirical mode decomposition (EMD), the Sparrow Search Algorithm (SSA), and BiLSTM, is proposed for long-term degradation forecasting. Specifically, EMD decomposes the hybrid HI into several intrinsic mode functions (IMFs) and a residual component with different time-scale characteristics, enabling the degradation features of PEMFCs to be captured more effectively. Each decomposed component is then modeled separately by BiLSTM to improve prediction accuracy under limited training data. Finally, SSA is employed to optimize the hyperparameters of BiLSTM, thereby reducing the risk of overfitting and enhancing the robustness of the prediction model. The main contributions of this paper are summarized as follows:

(1) A hybrid health indicator (HI) is constructed by integrating stack voltage and polarization resistance extracted from EIS data through the RC-RLQ equivalent circuit model. By combining system-level performance and component-level electrochemical degradation information, the hybrid HI provides a more comprehensive representation of PEMFC degradation under static and dynamic conditions.
(2) An EMD-based multi-scale feature extraction strategy is designed to decompose the hybrid HI into intrinsic mode functions and residual components, allowing global degradation trends and local fluctuations to be

captured from limited aging data.

(3) An SSA-optimized BiLSTM fusion ahead prediction method is developed for multi-step degradation prediction and RUL estimation. SSA reduces hyperparameter tuning complexity and overfitting risk, while component-wise prediction and fusion enable accurate 6-step and 10-step ahead forecasting.

The structure of this paper is shown as follows: Section 2 describes the implementation plan of the proposed fusion ahead decay prediction method. Section 3 presents the extraction and construction of the hybrid HI. Sections 4.1–4.3 introduce the EMD, BiLSTM and SSA methodologies, respectively. Section 5 presents the performance verification and experimental results of the proposed method. Section 6 concludes the paper.

2. The Implementation Plan of a Fusion Ahead Decay Prediction Method

2.1. Problem Formulation

The limited useful lifetime is a critical factor restricting the commercialization of PEMFC on a large scale. The PEMFC's four subsystem aging factors of air, hydrogen, hydrothermal, and electrical control accelerate the decay of the stack during the operation. The decay factors of the air and hydrogen subsystems are mainly the aging failure of key PEMFC components (such as clogged air filters, circulation pump failures), which will not be discussed here since those do not involve energy management. The energy management strategy of PEMFC mainly consists of hydrothermal management and electrical control strategy [22]. The PEMFC hydrothermal power decay factors and maintenance methods are specified in Table 1.

Table 1. PEMFC System-level decay factors and maintenance measures.

Subsystem Parts	Decay Factors	Influence	Reversibility	Maintenance Measures
Hydrothermal	Water pump failure	Difficulty in dissipating heat; causes drying of membrane	Reversible	Regular maintenance; fault tolerant control
	Membrane drying	Performance decay, membrane tearing	Irreversible if membrane cracking	reasonable hydrothermal management algorithm; Self-humidifying design strategy
	Membrane flooding	Performance decay, carbon corrosion and reverse polarity	Reversible if handled in time	Impulse gas exhaust control; change membrane material
Electronic control	Circuit overvoltage	Speeding carbon corrosion and catalyst solubilization	Reversible only in a short time	Regular maintenance of control algorithm and electronic devices
	Short circuit overvoltage	Membrane flooding; temperature rises suddenly	Reversible only in a short time	Insulation test and maintenance regularly
	Not real-time calibrated	Electricity demand and supply mismatch	Reversible in a short time	Regular calibration of controller parameters

Prognostic and Health Management (PHM) is a precautionary measure that has been widely proven to improve the RUL of PEMFC. Decay prediction and energy management strategies (EMS) correspond to prognostics and health management in PHM respectively. Decay prediction can provide future PEMFC operation state information, which provides theoretical basis and information support for the management, maintenance and decision-making of the PEMFC system. The EMS of PEMFC mainly consists of hydrothermal management and electrical control strategy. Advanced control strategies are effective in avoiding component failures and slowing down PEMFC aging.Lebreton et al. [23] proposed an online diagnosis of FC hydrothermal management fault problems with a neural network tool based on a calibrated PID controller. Chunchun Jia et al. [24] propose a novel cost-minimizing EMS to reduce the FC aging rate by 34.8%.

In addition, designing energy management strategies that are adaptive control to the parameters can greatly reduce the rate of decay of the PEMFC. Qi Li et al. [25] proposed a real-time EMS that can maximize the reduction of PEMFC operating cost. The experimental results show that the FC1 voltage decays only 0.94 $\mu V/h$ with EMS, where voltage decay is much lower than the power following strategy and H_2 minimization method. Fei Peng et al. [26] propose an improved EMS for PEMFC based on fuzzy logic hysteresis state machine. The voltage decay rate of PEMFC using improved EMS after 3744 h is 7.5 $\mu V/h$, which is lower than the voltage decay rate of 11.6 $\mu V/h$ in the literature [27].

The volatility of the output voltage of the PEMFC under dynamic working conditions can cause uneven degradation of the performance of the electrostack, thus affecting the overall durability of the PEMFC. The output voltage of the PEMFC fluctuates based on dynamic changes in load current, and these fluctuations may mask the true picture of PEMFC performance degradation. The limited training data results in predictive models that cannot adequately capture the intrinsic patterns and trends in the data and can result in overfitting or underfitting of the model. Therefore, a single HI and limited training data lead to inaccuracies in the prediction of long-term PEMFC decay. The detailed information on real static and dynamic PEMFC durability test data over 1000 h used in this paper can be found in reference [27].

PEMFC decay prediction is a key prerequisite for the realization of PHM technology and can provide effective scientific information for EMS development. The volatility of the output voltage of the PEMFC under dynamic working conditions can cause uneven degradation of the performance of the electrostack, thus affecting the overall durability of the PEMFC. The output voltage of the PEMFC fluctuates based on dynamic changes in load current, and these fluctuations may mask the true picture of PEMFC performance degradation. The limited training data results in predictive models that cannot adequately capture the intrinsic patterns and trends in the data and can result in overfitting or underfitting of the model. Therefore, a single HI and limited training data lead to inaccuracies in the prediction of long-term PEMFC decay. The detailed information on real static and dynamic PEMFC durability test data over 1000 h used in this paper can be found in reference [27].

2.2. PEMFC Fusion Decay Prediction Framework

The volatility of voltage under dynamic working conditions of PEMFC can easily result in the transitional accumulation of errors in the iterative prediction process of existing methods, which leads to inaccurate prediction results. Voltage as a static HI in the decay prediction of PEMFC also needs to consider the effect of various uncertainties (such as load changes, environmental factors, operational factors) on the output voltage. These uncertain factors have a certain degree of randomness, which results in inaccurate long-term prediction. Figure 1 presents the overall workflow of the proposed hybrid-health-indicator-based fusion ahead prediction framework. The framework is organized into five sequential stages: hybrid HI extraction, EMD-based multi-scale decomposition, SSA-based hyperparameter optimization, BiLSTM-based component prediction, and final fusion prediction. The key logic of this framework is that degradation representation is first improved before the prediction model is developed. Specifically, polarization resistance is extracted from EIS data using the RC-RLQ equivalent circuit model and is combined with stack voltage to construct the hybrid HI. Then, EMD decomposes the hybrid HI into multiple components with different time-scale characteristics, allowing the prediction model to capture both global degradation trends and local fluctuations. Finally, SSA optimizes the key hyperparameters of BiLSTM to reduce model complexity and mitigate overfitting under limited data. Therefore, Figure 1 is not only a flowchart of the algorithm but also illustrates the complete technical route from degradation indicator construction to long-term fusion prediction.

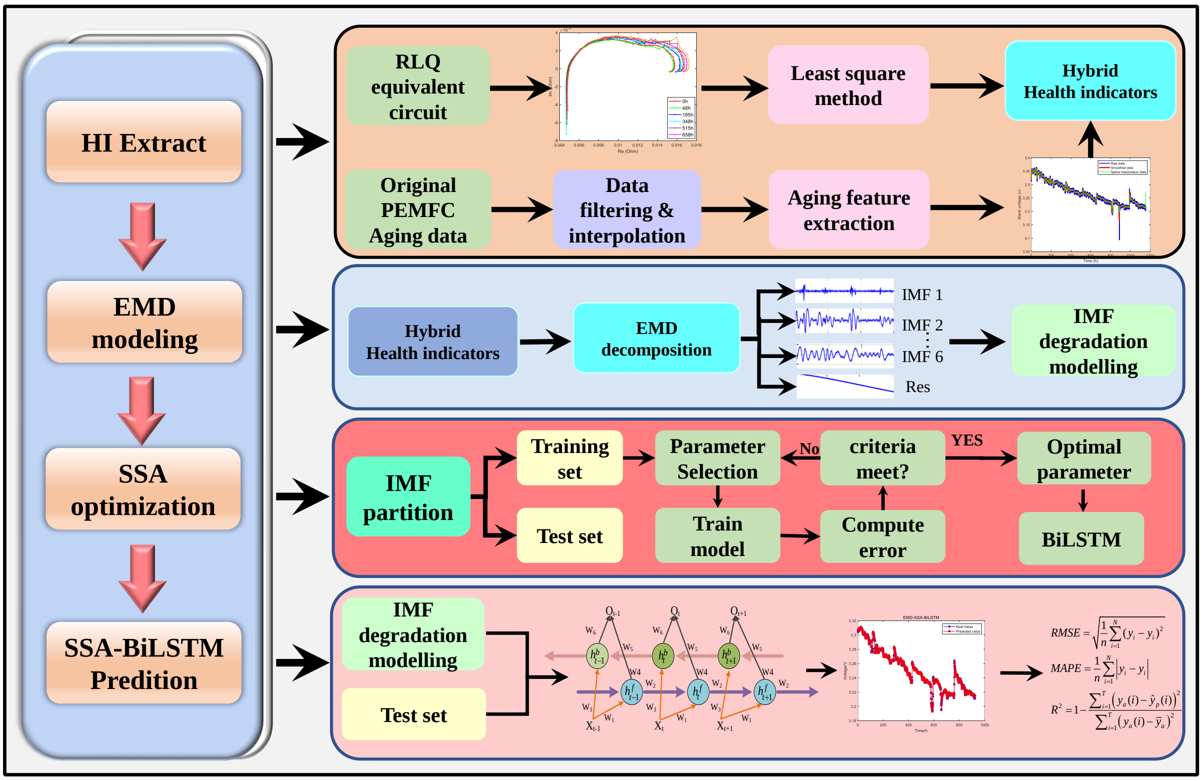

Figure 1. The structure and implementation process of the proposed EMD-SSA-BiLSTM model.

(1) HI Extract. An RC-RLQ equivalent circuit equation is proposed to extract the polarization resistance from the EIS data and form a hybrid HI with the voltage. Hybrid HI can accurately reflect the degradation of the PEMFC from the system level and component level under full operating conditions. The more technical details of Hybrid HI are described in Section 3.

(2) EMD modeling. EMD decomposes the hybrid HI to obtain multiple IMFs, which highlight the local characteristics of voltage data and polarization resistance at different time scales. EMD can smooth nonlinear aging data and increase the input features of prediction models under limited data. The more technical details of EMD are described in Section 4.1.

(3) The BiLSTM prediction model is established separately for each IMF to capture the decaying trend of the input HI over time and reduce prediction errors under limited data. A detailed description of the implementation of BiLSTM is presented in Section 4.2.

(4) Hyperparameters optimization with SSA. The hyperparameters of BiLSTM are optimized through SSA to reduce the computational complexity of the model and avoid BiLSTM overfitting. A detailed description of the implementation of SSA is presented in Section 4.3.

(5) Fusion method prediction. Finally, the prediction results are output after superimposing the prediction values of each model.

3. HI Extraction

In this section, polarization resistance is extracted from PEMFC electrochemical impedance spectroscopy (EIS) data by constructing an RC-RLQ equivalent circuit model. The relationship between stack voltage and polarization resistance is then examined using least-squares fitting and Pearson correlation analysis. Based on the complementary degradation information provided by these two variables, a hybrid health indicator (HI) is established by integrating stack voltage and polarization resistance.

The motivation for constructing the hybrid HI lies in the limitation of using voltage alone to characterize PEMFC degradation under dynamic operating conditions. Stack voltage reflects the external output performance of the PEMFC, but it is easily affected by load variations, operating condition changes, and local fluctuations, which may obscure the intrinsic degradation trend. In contrast, polarization resistance is more closely related to internal electrochemical degradation, including activation loss, mass-transfer limitation, and reaction resistance increase during aging.

Therefore, voltage and polarization resistance provide complementary information for degradation characterization. Voltage describes the system-level performance decay, whereas polarization resistance reflects the component-level electrochemical degradation state. The hybrid HI is defined as a two-dimensional time series:

$$H(y) = ((V_1, Z_1), (V_2, Z_2), \cdots, (V_y, Z_y)),$$

where $H(y)$ denotes the hybrid HI up to the y-th time period, and (V_y, Z_y) represents the stack voltage and polarization resistance at the y-th time period. By coupling these two indicators, the hybrid HI provides a more comprehensive and physically interpretable representation of PEMFC degradation.

3.1. The Principle Description of the RC-RLQ Equivalent Circuit Model

The EIS obtains the impedance response data of the PEMFC by introducing AC signals of different frequencies. As shown in Figure 2, the EIS curve of the PEMFC usually consists of two semicircles and an arc below the real axis at the low-frequency signals and a long arc at the high-frequency signals. The intersection of the impedance curve with horizontal axis characterizes the Ohmic resistance (OR) of the PEMFC. The real part of the impedance of the PEMFC varies very little by the external inductance in the green vertical region of the high frequency of Figure 2, but the imaginary part extends longer in the negative region. Thus the RC-RLQ equivalent circuit region A consists of an external inductor $L1$ in series with an ohmic resistor $R1$. Anode losses are ignored since it have a small effect on the impedance. Regions 2 and 3 in Figure 2 are characterized as cathode activation polarization loss (CAPL) and concentration polarization loss (CPL) for the PEMFC, respectively. The CAPL and CPL in Figure 2 are both circular arcs in positive number interval, so CAPL and CPL can be replaced by using two RC equivalent circuits in parallel, respectively. The double-layer capacitance C_1 characterizes the equivalent capacitance formed by the electrode and electrolyte, and R_2 is the polarization resistance that characterizes the strength of the redox reaction. The equivalent circuit of C_1 and R_2 in parallel to characterize the CAPL. The RLC equivalent circuit consisting of reactant diffusion resistance $R3$, reactant solubility inductance L_2, and parallel double layer capacitance C_2 characterizes the electronic and proton conduction procedures at the CPL. Since the surface roughness of the

PEMFC porous electrode and the current density are not uniformly distributed along the length of the hole, there will be a concave portion between the two semicircles of the actual EIS. In this paper, constant-phase element CPE is used instead of C_2 to emulate the deformation of impedance arc resulting from inhomogeneous surface dispersion of porous electrodes. CPE is represented by Q in the EIS fitting software ZView. The total impedance equation for the PEMFC calculation based on the equivalent circuit diagram of Figure 3 is as follows:

$$Z = R_1 + jwL_m + \frac{1}{\frac{1}{R_2} + jwC_2} + \frac{1}{\frac{1}{R_3} + \frac{1}{JwL_2} + Q(jw)^{\varphi}}. \tag{1}$$

where φ is the index of CPE, and ω is the EIS test frequency. When the frequency ω is 0, Z_r denotes the polarization resistance of the PEMFC.

$$Z_r = R_1 + R_2. \tag{2}$$

ZView software is widely applied to the processing and impedance fitting of EIS data from PEMFC. The RC-RLQ equivalent circuit is developed in ZView software to fit the EIS data at different moments. The parameters of the equivalent circuit model are iteratively resized using the ZView's inbuilt mathematical algorithms to make the models' predictions close to the experimental data. Once the ZView fit is complete, the user analyzes whether the fit matches the real data. If the fitting results does not match the real data, the initial parameters are readjusted to obtain a better fit result. The Figure 3 also proves that the fitted EIS curves are very close to the actual EIS curves.

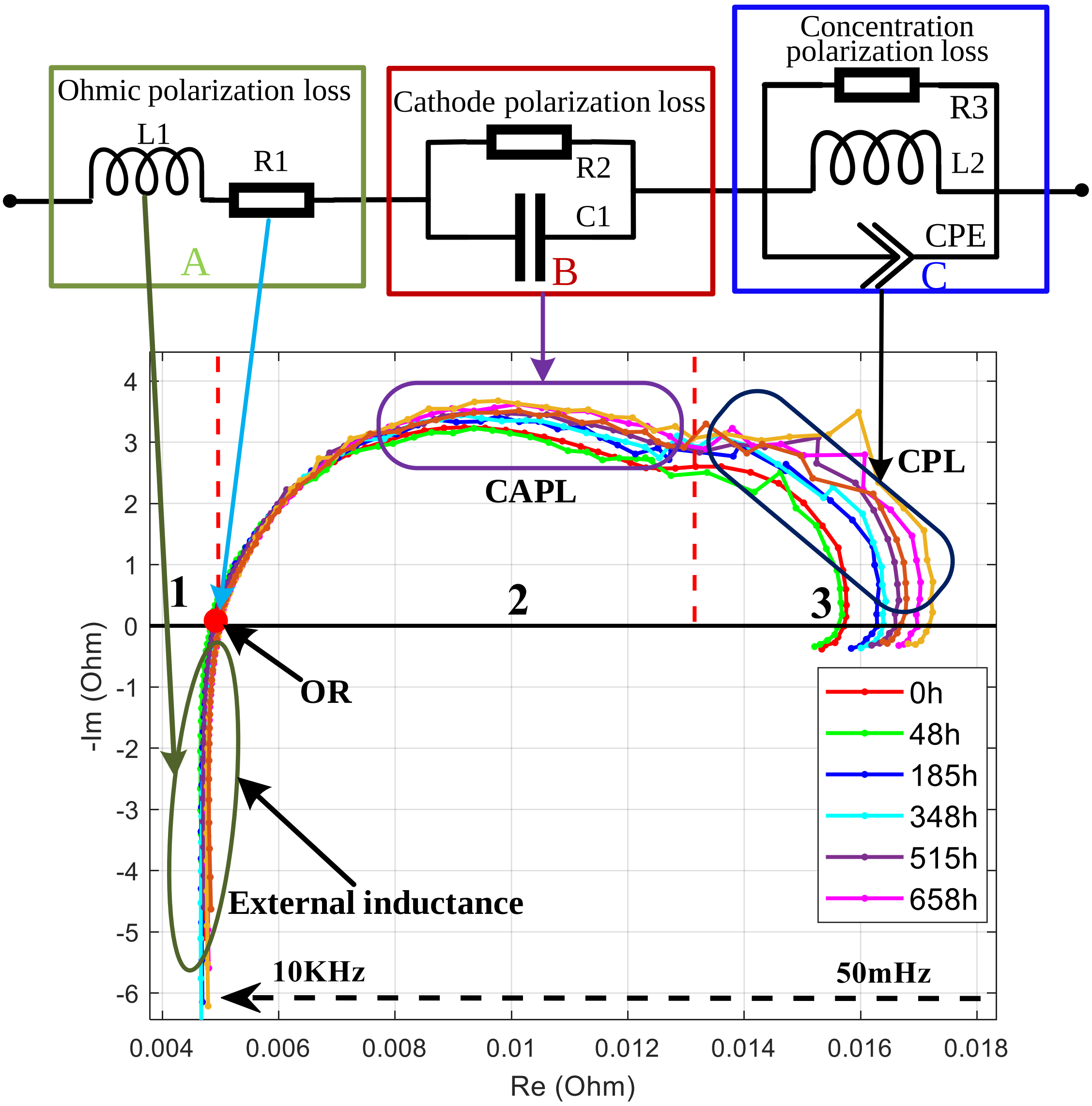

Figure 2. The RC-RLQ equivalent circuit model based on Nyquist diagram of EIS.

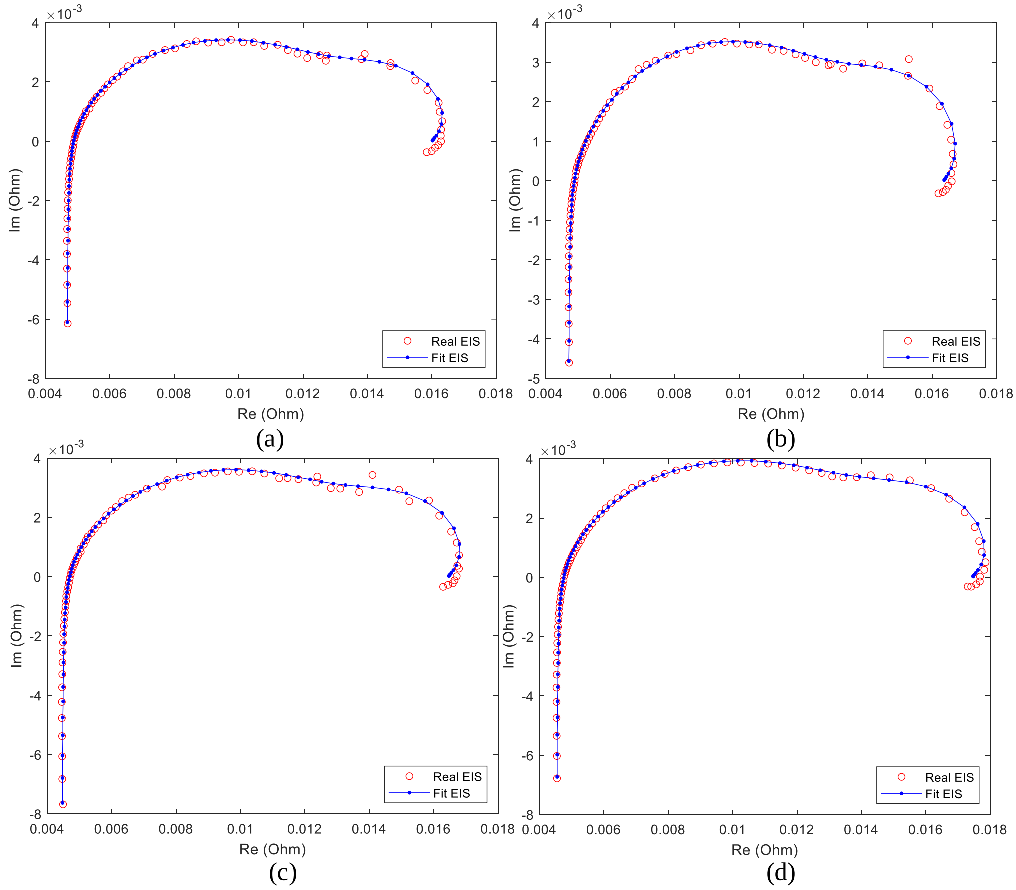

Figure 3. Fitting EIS curve of PEMFC (**a**) FC1-185 h; (**b**) FC1-515 h; (**c**) FC2-182 h; (**d**) FC2-515 h.

3.2. Calculation of Polarization Resistance

The data for static and dynamic working conditions in the PEMFC real durability test dataset are referred to as FC1 and FC2, respectively. The fitting results of the RC-RLQ equivalent circuit model for polarization impedance at FC1 and FC2 are shown in Table 2.

Table 2. Equivalent circuit parameters for FC1 and FC2 datasets.

Datasets	Time	R1	R2	Z_r
FC1	T048	0.00463	0.01074	0.01537
	T185	0.004648	0.01137	0.016018
	T348	0.004656	0.01152	0.016176
	T515	0.004681	0.01169	0.016371
FC2	T035	0.004389	0.01155	0.015939
	T182	0.004436	0.01203	0.016466
	T343	0.00445	0.01223	0.01668
	T515	0.004519	0.01294	0.017459

The data points $((U_1, R_1), (U_2, R_2), \cdots, (U_n, R_n))$ of the voltage (U) and the polarization resistor (R) can be fitted linearly by the least squares method. Define the residual of the vertical coordinate $\hat{\varepsilon}_i$ as the difference between the actual value and the fitted value ,and the specific formula for the residual is shown as follows:

$$\hat{\varepsilon}_i = R_i - \hat{R}_i. \tag{3}$$

To minimize the slope error of the fit, which means finding a set of slope k with intercept c that minimizes the value of the objective function. The objective function of the least squares method is defined as follows:

$$J(k, c) = \sum\nolimits_{i=1}^{n} \hat{\varepsilon}_i^2 = \sum\nolimits_{i=1}^{n} (\hat{r}_i - r_i)^2 = (\hat{\mathbf{r}}_i - \mathbf{r_i})^T (\hat{\mathbf{r}}_i - \mathbf{r_i}). \tag{4}$$

where $\widehat{r} = [\hat{r}_1, \hat{r}_2 \cdots, \hat{r}_n]$, $r = [r_1, r_2, \cdots, r_n]$. The partial derivatives of k and c of $J(k,c)$ and the specific formulas of k and c are as follows:

$$\begin{aligned} \frac{\partial J(k,c)}{\partial k} &= 2\sum_{i=1}^{n} u_i(ku_i + c - r_i)^2 = 0 \\ \frac{\partial J(k,c)}{\partial c} &= 2\sum_{i=1}^{n} u_i(ku_i + c - r_i)^2 = 0 \end{aligned} \tag{5}$$

$$k = \frac{\sum_{i=1}^{n} r_i(u_i - \overline{u})^2}{\sum_{i=1}^{n} {u_i}^2 - \frac{1}{n}(\sum_{i=1}^{n} u_i)^2}. \tag{6}$$

$$c = \frac{1}{n}\sum_{i=1}^{n}(r_i - ku_i). \tag{7}$$

Figures 4 and 5 provide statistical evidence for constructing the proposed hybrid health indicator. Figure 4 shows that voltage and polarization resistance exhibit an approximately linear relationship in both FC1 and FC2 datasets. This indicates that polarization resistance evolves consistently with the voltage degradation process. Figure 5 further quantifies this relationship using Pearson correlation analysis. The results show that voltage and polarization resistance are strongly negatively correlated in both datasets. As PEMFC aging proceeds, the stack voltage gradually decreases, while the polarization resistance increases. This opposite but consistent variation trend indicates that polarization resistance can supplement voltage by providing internal electrochemical degradation information. Therefore, Figures 4 and 5 jointly support the rationality of coupling voltage and polarization resistance as a hybrid health indicator.

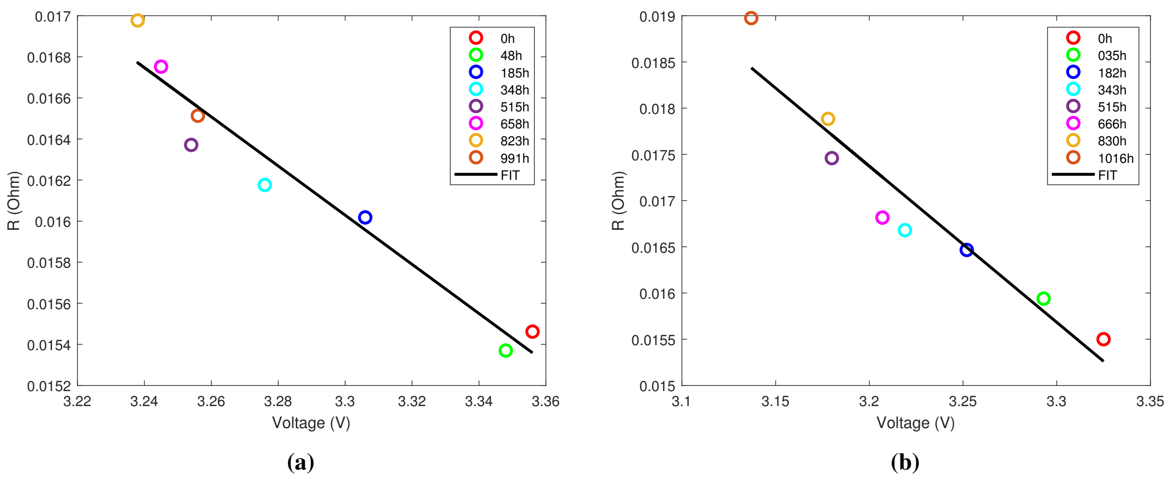

Figure 4. Linear fitting results between voltage and polarization resistance: (**a**) FC1; (**b**) FC2.

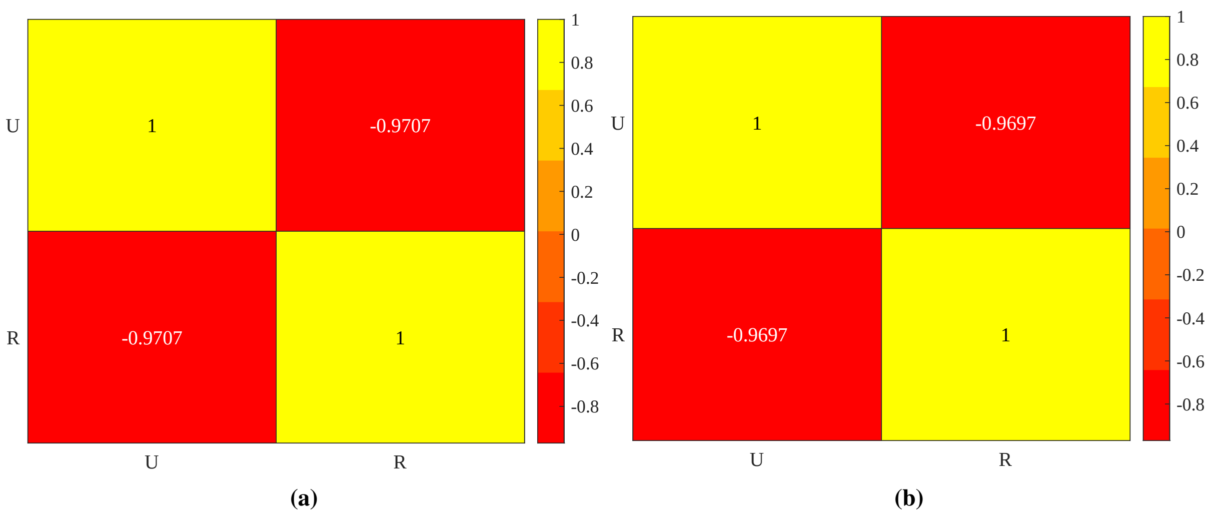

Figure 5. The Pearson correlation coefficient results of voltage and polarization resistance (**a**) FC1; (**b**) FC2.

4. Fusion Prognostic Framework Based on EMD and SSA-BiLSTM

4.1. Hybrid HI Empirical Mode Decomposition

The EMD decomposes the voltage and polarization resistance into totaling 12 IMF and 2 residuals. The input features of BiLSTM are increased from two inputs (Hybrid HI) to 12 inputs (IMF) after EMD. Each IMF has all the information the fluctuations of the original data on the corresponding time scale. The EMD decomposition of Hybrid HI is processed as follows:

(1) Find all the extreme points of hybrid HI $H(y)$ and plot the upper and lower envelopes of $H(y)$ using cubic spline interpolation. Denote the upper and lower envelopes as $e_{\max}(y)$ and $e_{\min}(y)$ respectively.

(2) The mean envelope is drawn from the mean of the upper and lower envelopes and is denoted as t_y.

$$t_y = \frac{e_{\max} + e_{\min}}{2} \tag{8}$$

(3) The original data $H(y)$ is used to subtract the mean $t(y)$ to obtain the data $d(y)$.

(4) Determine whether $d(r)$ satisfies the 2 constraints of the IMF, if so, $d(r)$ is the decomposed IMF and is denoted as $w(r)$; if not, repeat steps 1 to 4 based on $d(r)$. The residual term $R(r)$ is as follows:

$$R(r) = H(y) - d(r). \tag{9}$$

(5) Repeat steps 1 to 4 k times until the residual $R(r)$ becomes a monotonic function or less than the preset error. The decomposition is complete.

$$H(y) = \sum_{j=1}^{k} w_j(r) + R(r). \tag{10}$$

The hybrid HI sequence is decomposed into 6 IMFs and 1 Residual from high to low frequency by EMD. The 6 IMFs reflect the distribution of PEMFC voltage data over different influences and different time scales, from normal stack decay to fault voltage.

4.2. BiLSTM Principle Architecture

BiLSTM is a variant of LSTM that captures forward and backward contextual information of sequence data by adding a reverse LSTM layer. The basic structure of an LSTM consists of input gates, forget gates, output gates, and a cell state, and together these components control the flow and storage of information in the cell. The internal state memory unit that stores long-term information in the LSTM at time t is c_t.

The LSTM has 3 input data: the cell output h_{t-1} and the cell state c_{t-1} at the $t-1$ moment, as well as the input x_t at the t moment. The forgetting gate selectively extracts information or memory from the memory unit based on h_{t-1} and x_t. The LSTM formula can be expressed as follows:

$$f_t = \sigma(W_f \cdot [h_{t-1}, x_t] + b_f). \tag{11}$$

$$i_t = \sigma(W_i \cdot [h_{t-1}, x_t] + b_i). \tag{12}$$

$$\widetilde{c_t} = \tanh(W_c \cdot [h_{t-1}, x_t] + b_c). \tag{13}$$

$$c_t = f_t \cdot c_{t-1} + i_t \cdot \widetilde{c_t}. \tag{14}$$

$$o_t = \sigma(W_o \cdot [h_{t-1}, x_t] + b_o). \tag{15}$$

$$h_t = o_t \cdot \tanh(c_t). \tag{16}$$

where f_t, i_t and o_t are the outputs of the forget, input and output gates, respectively. c_t is the cell state, and $\widetilde{c_t}$ is the candidate cell state. W_f, W_i, W_o and W_c are the corresponding weight matrices, while b_f, b_i, b_o, and b_c are the corresponding bias vectors. The function $\sigma(\cdot)$ denotes the sigmoid activation function. and $\tanh(\cdot)$ denotes the hyperbolic tangent activation function.

The output result of BiLSTM is related to both forward and backward data, which fully utilizes the interaction of data and iteratively utilizes the weight parameters, reducing the requirement for raw data. The BiLSTM is shown in Figure 6, which differs from the LSTM structure by the addition of a back-propagation layer for the data.

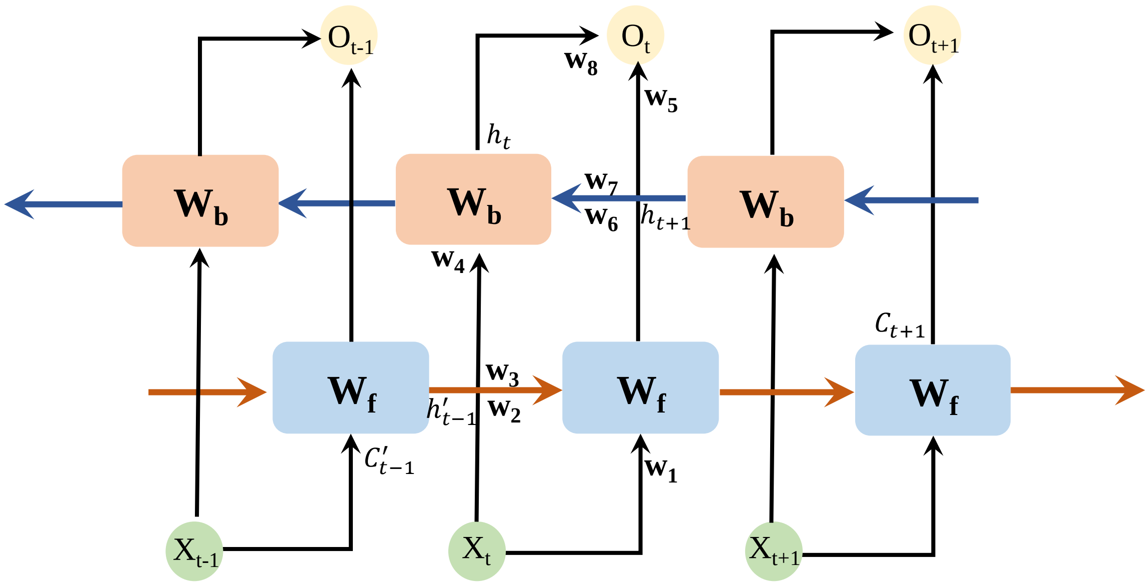

Figure 6. The structure of BiLSTM.

The output values are a weighted combination of forward and reverse data. Time series data of voltage are used as inputs. In Figure 6, W_f and W_b are the weights of the forward and reverse layers, respectively, and w_1–w_8 are the eight weight values that are reused at each moment of the BiLSTM. The output of BiLSTM is obtained by weighting and combining the outputs of both forward and backward networks to make decisions using both historical and future information from time series data, whose formula can be expressed as follows:

$$h'_t = \sigma\left(\omega_1 x_t + \omega_2 C'_{t-1} + \omega_3 h'_{t-1}\right). \tag{17}$$

$$h_t = \sigma\left(\omega_4 x_t + \omega_6 C'_{t-1} + \omega_7 h'_{t-1}\right). \tag{18}$$

$$o_t = \sigma\left(\omega_5 h'_t + \omega_8 h_t\right). \tag{19}$$

where h'_t and h_t are the outputs of the forward layer and the hidden layer at time t.

At each time step, the input sequences are fed into the forward and backward networks of BiLSTM in forward and backward order, respectively. The forward and backward networks capture the temporal features of the input data to obtain the hidden states of the forward and backward networks, respectively. The forward and backward hidden states are weighted and combined to obtain the final hidden state h_t^{final}. The weighted combination usually uses a learnable weight α to adjust the contribution of the forward and backward hidden states. The specific weighted combination formula is as follows:

$$h_t^{final} = \alpha \cdot h_t^{forward} + (1-\alpha) \cdot h_t^{backward} \tag{20}$$

where $h_t^{forward}$ is the hidden state of the forward LSTM network at time step t, $h_t^{backward}$ is the hidden state of the backward LSTM at time t. α is a learnable weight that is updated via backpropagation during training process. α controls the contribution of the forward and backward hidden states to the final hidden state. α allows the model to learn the optimal combination according to the task. The final hidden state h_t^{final} is fed into the output layer to obtain the predicted value at time step t.

4.3. Swarm Search Algorithm

SSA has the advantages of fast convergence and not falling into local optimum. The learning rate, the epochs and the number of neurons of the BiLSTM network are the key parameters that affect the prediction accuracy. These parameters directly determine the network structure of the BiLSTM model, and the prediction accuracies of models trained using different parameters vary greatly. Therefore, the number of neurons, learning rate, and training times of the BiLSTM hidden layer are optimized through SSA. Individuals in a sparrow colony are classified into two types based on their behavior: Producers and Scroungers. Producers are responsible for exploring for food and informing other sparrows of the location of the food found. The Scroungers, on the other hand, forage for food by following the Producers. Some individuals in a sparrow colony are endowed with the behavior of sensing danger, and these sparrows are called vigilantes. When the vigilantes perceive danger, the entire colony abandons its foraging and takes precautions. In short, sparrow colonies improve foraging efficiency and safety through division of labor and vigilance mechanisms. In the $(t+1)$-th iterations, the location of the producers is updated as follows:

$$X_{i,j}^{t+1} = \begin{cases} X_{i,j}^{t} \cdot \exp\left(-\frac{i}{a \cdot T}\right) & R_2 < S \\ X_{i,j}^{t} + Q \cdot L & R_2 \geq S \end{cases} \tag{21}$$

where $X_{i,j}^{t}$ is the position of the i-th sparrow in dimension j at iteration t . The variable a represents a random number uniformly distributed between 0 and 1. The warning value R_2 varies from 0 to 1, which indicating the degree of perceived danger, while the safety value S ranges from 0.5 to 1, which representing the level of safety measures implemented by the colony. The variable Q follows a normal distribution. L is a matrix with dimensions 1 by d.

When $R_2 < S$, it signifies that the environment is safe, prompting the Producers to continue their search for food. However, if $R_2 \geq S$, it indicates that predators have been detected, prompting the sparrow population to abandon their foraging activities and relocate to safer areas. In such cases, the formula for updating the Scroungers' positions is as follows:

$$X_{i,j}^{t+1} = \begin{cases} Q \cdot \exp\left(\frac{X_{\text{worst}} - X_{i,j}^{t}}{t^2}\right) & i > \frac{n}{2} \\ X_p^{t+1} + \left|X_{i,j}^{t} - X_p^{t+1}\right| \cdot A^{+} \cdot L & \text{otherwise} \end{cases} \tag{22}$$

Where X_p represents the current optimal position of the Producers and X_{worst} denotes the worst position, A is a 1 × d matrix with elements randomly set to 1 or -1, and A^{+} is the pseudo-inverse of A calculated as $A^T(AA^T)^{-1}$. If i exceeds half of the total population size, it signifies that the ith Scrounger is experiencing starvation, characterized by a lower fitness value. To enhance the survival rate against predators, it's crucial to seek food in alternative locations. When danger is detected by the vigilantes, anti-predation behavior ensues, which is expressed by the following:

$$X_{i,j}^{t+1} = \begin{cases} X_{best}^{t} + \beta \cdot \left|X_{i,j}^{t} - X_{best}^{t}\right| & f_i > f_g \\ X_{i,j}^{t} + K \cdot \left(\frac{\left|X_{i,j}^{t} - X_{best}^{t}\right|}{(f_i - f_w) + \varepsilon}\right) & f_i = f_g \end{cases} \tag{23}$$

where X_{best} represents the global optimal position of the SSA. β serves as a control parameter for adjusting step size. The variable K is a random variable within the range of -1 to 1. f_g and f_w represent the best and worst fitness values, respectively. ε is a constant introduced to prevent division by zero. f_i represents the fitness value of the current sparrow. If f_i exceeds f_g, it indicates that the newly recruited sparrow is positioned at the outer limit of the sparrow population. Conversely, if f_i equals f_g, it indicates that the newly recruited sparrow has detected danger, prompting the Producers to initiate the next round of search.

5. Results and Discussion

5.1. The Multistep Decay Prediction of PEMFC

The comparison results of predictions between the fusion ahead prediction method and LSTM, BiLSTM, and ESN on the 185 h training data of the FC1 dataset are shown in Figure 7a and Table 3. The 6-step prediction of ESN using 185 h training data deviates from the trend of true decay, and the predicted values kept increasing with time. The 6-step prediction results of BiLSTM and LSTM reflected the decay trend of PEMFC to some extent, but the predicted values had large errors with the real values. The multistep predicted values of the FAPM in this paper are in general agreement with the true values, and it is demonstrated that the method is able to precisely forecast the detailed decay of the PEMFC under static working conditions. The root mean squared error (RMSE), mean absolute error (MAE) and coefficient of determination (R_2) of the fused ahead prediction method for the FC1-185 h training data are 0.00227, 0.00166 and 0.9387, respectively.

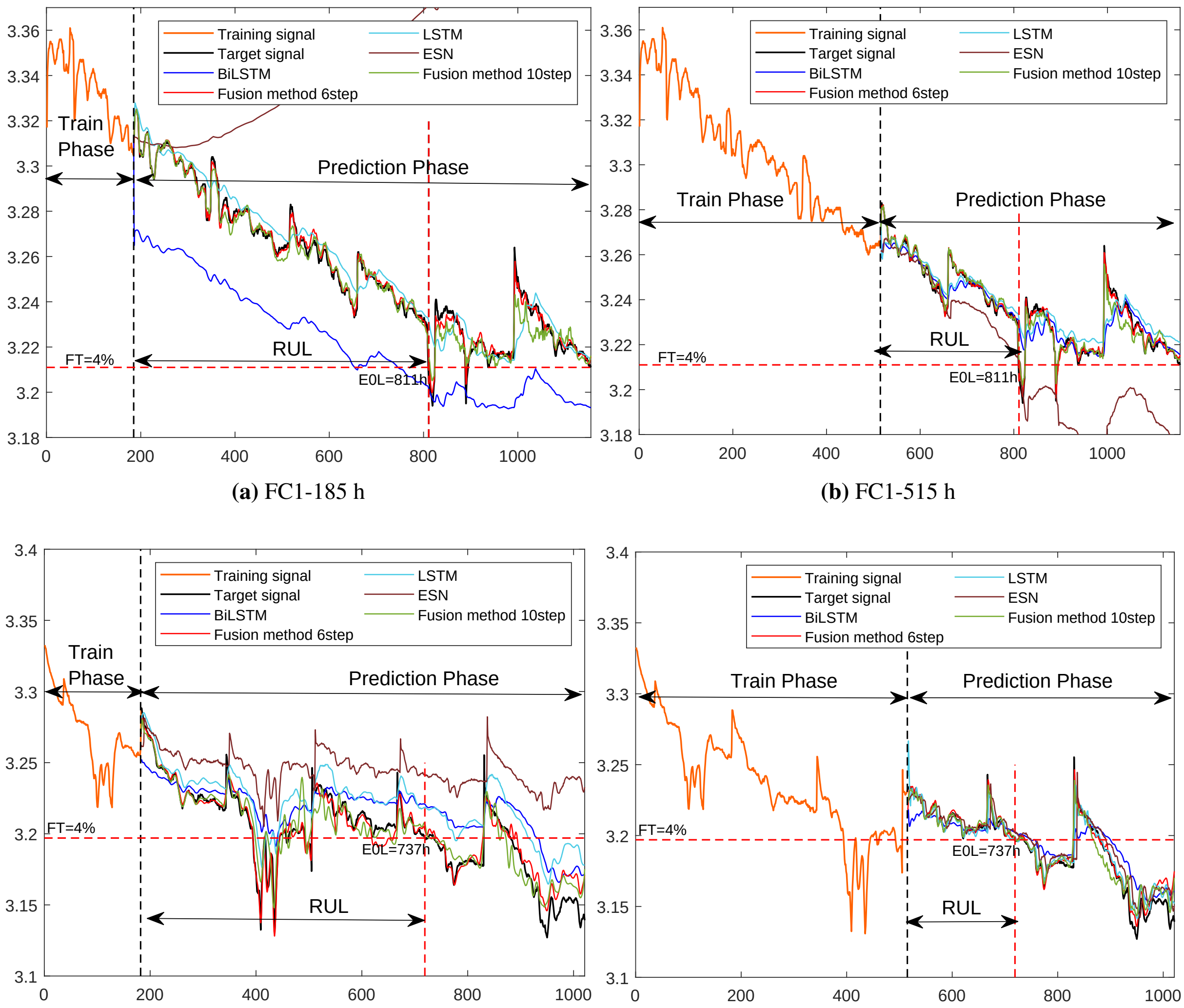

(a) FC1-185 h (b) FC1-515 h

(c) FC1-182 h (d) FC1-515 h

Figure 7. Multi-step PEMFC decay results of fusion ahead prediction methods (**a**) 185 h-FC1; (**b**) 515 h-FC1; (**c**) 182 h-FC2; (**d**) 515 h-FC2.

Table 3. Comparison of experimental results of four models

Dataset	Index	LSTM	BiLSTM	ESN	Fusion Method 6-step	Fusion Method 10-step
FC1-185 h	RMSE	0.0084	0.0332	0.1288	0.0023	0.0046
	MAE	0.0063	0.0320	0.1066	0.0017	0.0075
FC1-515 h	RMSE	0.0082	0.0076	0.0294	0.0015	0.0032
	MAE	0.0060	0.0047	0.0237	0.0011	0.0043
FC2-182 h	RMSE	0.0227	0.0221	0.0488	0.0080	0.0104
	MAE	0.0190	0.0185	0.0441	0.0055	0.0075
FC2-515 h	RMSE	0.0070	0.0130	0.0108	0.0054	0.0064
	MAE	0.0043	0.0096	0.0075	0.0033	0.0043

The RMSE and MAE of the three compared algorithms decreased with the increase training set to 515 h. However, the predicted values still had large errors with the real data, which could not precisely reflect the short-term decay and fluctuation behavior of PEMFC. The predicted values of the FAPM using hybrid HI under different training are highly consistent with the real decay data. The minimum value of R_2 by the 6-step prediction for fusion advance prediction method is 0.9387, which indicates that the method can precisely predict the static decay behavior of PEMFC with limited data.

Figure 7 and Table 3 compare the multi-step prediction performance of the proposed fusion ahead prediction method with LSTM, BiLSTM, and ESN. Under the dynamic FC2-182h condition, the output voltage fluctuates significantly due to load current variation, making long-term multi-step prediction more challenging. Although LSTM and BiLSTM can capture the overall degradation trend, their prediction curves tend to be overly smooth and cannot accurately describe sharp local degradation fluctuations. ESN shows larger deviations from the true degradation trajectory. In contrast, the proposed fusion ahead prediction method maintains better agreement with the true degradation curve under both 6-step and 10-step prediction settings. With only 182 h of training data in the FC2 dataset, the proposed 6-step method achieves an RMSE of 0.0080 and an MAE of 0.0055, which are lower than those of LSTM, BiLSTM, and ESN. These results indicate that the hybrid HI and EMD-SSA-BiLSTM fusion framework can improve the robustness of PEMFC long-term degradation prediction under limited dynamic data. The minimum R_2 value of 0.8813 for the fusion prediction method, which demonstrates it has efficient and accurate multi-step prediction performance of using the hybrid HI fusion prediction algorithm.

With the FC1-185 h and FC2-182 h training set, the RMSE and MAE of the fusion prediction method for 6-step and 10-step predictions are lower than those of the three comparison methods. The forecast error of multi-step prediction accumulates as the number of steps increases. The 10-step fusion ahead prediction method has slightly higher RMSE and MAE than the 6-step ahead prediction fusion prediction method. And 10-step prediction local PEMFC decay prediction curve is smoother and the accuracy decreases. Increasing the step length of the fusion prediction method will increase the error accordingly, but a longer prediction step is more meaningful for the PHM of PEMFC, therefore the increased error is acceptable.

A model based on the Bayesian framework and model and state simultaneous estimation (Bayes-MUSE) approach is proposed in [28] to quantify the aging of the PEMFC. The mechanism-based prediction methods such as Bayes-MUSE, Extended Kalman Filter (EKF), Unscented Kalman Filter (UKF) and Unscented Particle Filter (UPF) are selected for comparative experiments with fusion ahead prediction methods. Comparative experiment using IEEE 2014 PEMFC open-source data, with the same training data employed for comparative experiments. UKF is an empirical based model, UPF, EKF and Bayes-MUSE are mechanistic based model, and EMD-SSA-BiLSTM is data-driven based model. The RMSE and Mean Absolute Percentage Error (MAPE) are used to quantify the prediction performance of the five methods, and the results of the comparison experiments are presented in Table 4.

The comparison results show that the RMSE and MAPE of single-step and multi-step prediction of fusion ahead prediction method use hybrid HI are below the four comparison methods under FC1 and FC2 dataset. The results demonstrate that the prediction properties of the FAPM outperform both the empirical and mechanistic modeling methods.

Table 4. Comparative results of the proposed method with empirical and physics-based models

Indicator	Algorithm	FC1-Dataset				FC2-Dataset			
		50%	60%	70%	80%	50%	60%	70%	80%
RMSE	EKF	0.015	0.018	0.029	0.029	0.043	0.033	0.023	0.024
	UKF	0.027	0.019	0.037	0.021	0.026	0.018	0.019	0.023
	UPF	0.018	0.016	0.020	0.023	0.027	0.035	0.024	0.033
	Bayes-MUSE	0.014	0.014	0.015	0.021	0.016	0.017	0.018	0.023
	Proposed Method	0.0009	0.0006	0.0007	0.0006	0.0024	0.0020	0.0024	0.0024
	Proposed Method 6-step	0.0009	0.0007	0.0008	0.0007	0.0027	0.0030	0.0033	0.0042
MAPE	EKF	0.004	0.004	0.007	0.008	0.011	0.008	0.005	0.006
	UKF	0.006	0.005	0.009	0.006	0.006	0.004	0.005	0.006
	UPF	0.004	0.004	0.005	0.007	0.007	0.010	0.007	0.009
	Bayes-MUSE	0.003	0.003	0.004	0.005	0.004	0.004	0.004	0.005
	Proposed Method	0.0002	0.0001	0.0001	8.79×10^{-5}	0.0004	0.0003	0.0004	0.0003
	Proposed Method 6-step	0.0002	0.0001	0.0002	0.0002	0.0003	0.0005	0.0007	0.0007

5.2. The Ablation Experiment

The polarization resistance estimated from each EIS test cannot be directly applied to real-time prediction since EIS can only be tested after the PEMFC is offline. But as shown in Table 2, the polarization resistance Z_r in the FC1 and FC2 datasets increases linearly with time. And the linear correlation between voltage and polarization resistance is proved and the fitting equation is obtained in Section III.B in the paper. The polarization resistance in the actual prediction process is therefore indirectly obtained by inputting the voltage into the fitting equation in real time. Therefore, the polarization resistance can be involved in the real-time assessment of the health status of the

PEMFC. The ablation experiments of input indicators are added in the paper to demonstrate the enhancement of the long-term decay prediction accuracy by hybrid HIs. The step size of the ablation experiment is set to 6. The experimental results in Table 5 demonstrate that the RMSE and MAE of the EMD-SSA-BiLSTM using hybrid HI are lower than those of the single-input indicator. The ablation experiment demonstrates that the addition of polarization resistance as an input indicator improves the long-term prediction precision of the model.

Table 5. Ablation experiment of input indicators

Train Data	HI	RMSE	MAE
FC1-185 h	U	0.0034	0.0025
	UR	0.0023	0.0017
FC1-515 h	U	0.0030	0.0021
	UR	0.0015	0.0011
FC2-182 h	U	0.0148	0.0099
	UR	0.0080	0.0055
FC2-515 h	U	0.0097	0.0073
	UR	0.0054	0.0033

Traditional prediction algorithms are prone to overfitting when the data is limited and the model is complex, resulting in low prediction accuracy. The EMD is used to increase input data, and SSA is used for automatic parameter optimization to reduce complexity in this paper. EMD and SSA can avoid BiLSTM from overfitting under limited data. The ablation experiment is added in this paper to demonstrate that EMD improves the forecasting precision by increasing the inputs to the prediction model with limited data. The total number of parameters (TNOP) for fixed-parameter BiLSTM under arbitrary training intervals for both static and dynamic datasets is 82,802. The RMSE, MAE and TNOP of SSA-BiLSTM are lower than those of BiLSTM under the datasets of both static and dynamic. The ablation experiment results in Table 6 demonstrate that SSA can reduce the computational complexity of BiLSTM network and thus improve the prediction accuracy. The RMSE, MAE and TNOP of the EMD-SSA-BiLSTM are lower than SSA-BiLSTM. Although EMD increases the complexity of BiLSTM networks, SSA parameter auto-optimization reduces the TNOP in BiLSTM. The smaller TNOP means lower model complexity and risk of overfitting.

Table 6. Ablation study of EMD and SSA.

Train Data	Method	RMSE	MAE	TNOP
FC1-185 h	BiLSTM	0.0187	0.017432	82,802
	SSA-BiLSTM	0.0073	0.0065	31,330
	Fusion method	0.0023	0.0017	7592
FC1-515 h	BiLSTM	0.0114	0.0093	82,802
	SSA-BiLSTM	0.0065	0.0056	67,354
	Fusion method	0.0015	0.0011	46,408
FC2-182 h	BiLSTM	0.0171	0.0131	82,802
	SSA-BiLSTM	0.0113	0.0101	57,446
	Fusion method	0.0080	0.0055	51,712
FC2-515 h	BiLSTM	0.0137	0.0102	82,802
	SSA-BiLSTM	0.0072	0.0059	41,840
	Fusion method	0.0054	0.0033	37,628

5.3. The RUL Accuracy Estimation

The output voltage at which the PEMFC decays to 96% is taken as the fault voltage threshold dose (TD), and its corresponding time is the end-of-life (EOL) time. The RUL comparative results of the four methods are shown in Table 7. The Err is introduced as a metric to evaluate the RUL precision of prediction model, and the specific equation for Err is presented below.

$$Err = \frac{|RUL_{\text{true}} - RUL|}{RUL_{\text{true}}} \times 100\% \tag{24}$$

where RUL_{true} and $\overline{RUL}$ are the true RUL and the model-predicted RUL of the PEMFC, respectively.

The complexity of the dynamic working conditions and the limited training set increase the difficulty of multi-step RUL prediction, which leads to the predicted values reaching the failure threshold earlier. The Err of the 6-step and 10-step RUL predictions of the fusion ahead prediction method is much lower than that of BiLSTM at only 0.33% and 0.63% when the training data is FC1-185 h. However, the ESN and BiLSTM predictions do not decay to the fault voltage under static operating conditions with limited data. The predicted values of ESN do not decay to the fault voltage when the training data is the first 182 h of FC2; The 6-step and 10-step prediction Err of this fusion prediction method under the FC2-182 h training data are 18.67% and 12.04%, respectively. Although the multi-step prediction values are advanced to reach the failure threshold resulting in larger errors, both prediction errors are far below those of LSTM and BiLSTM. The FAPM using hybrid HI achieves high prediction precision under FC2 dataset with multiple training data, and the minimum value of R_2 is only 0.8813. Compared with single-step prediction, the accuracy of 6-step and 10-step ahead prediction decreases, but 10 h ahead RUL prediction is very significant for PEMFC maintenance. The 6- and 10-step prediction results prove the superior long-term RUL prediction performance of the FAPM using hybrid HI under limited data.

Table 7. The RUL comparative experimental results of four methods.

Data Set	EOL	TD	Algorithm	Real RUL	Forecast RUL	Err	R_2
FC1	3.211 V	185 h	LSTM	625 h	——	——	0.9324
			BiLSTM		560.611 h	10.30%	0.9421
			ESN		——	——	−17.237
			Fusion method 6-step		627.071 h	0.33%	0.9387
			Fusion method 10-step		628.916 h	0.63%	0.7612
		515 h	LSTM	295 h	——	——	0.8214
			BiLSTM		——	——	0.8169
			ESN		299.125 h	1.40%	−1.811
			Fusion method 6-step		295.82 h	0.28%	0.9798
			Fusion method 10-step		298.068 h	1.04%	0.9177
FC2	3.197 V	182 h	LSTM	537 h	741.347 h	38.05%	0.9228
			BiLSTM		749.385 h	39.55%	0.8327
			ESN		——	——	−1.557
			Fusion method 6-step		436.747 h	18.67%	0.8813
			Fusion method 10-step		472.323 h	12.04%	0.7943
		515 h	LSTM	204 h	206.669 h	1.31%	0.9498
			BiLSTM		233.45 h	14.44%	0.8521
			ESN		234.425 h	14.91%	0.8358
			Fusion method 6-step		202.701 h	0.64%	0.9627
			Fusion method 10-step		202.959 h	0.51%	0.9426

6. Conclusions

This paper proposes a hybrid health indicator (HI) and an EMD-SSA-BiLSTM-based fusion prediction method for accurate PEMFC remaining useful life (RUL) prediction under dynamic degradation and limited data conditions. A second-order RC-RLQ equivalent circuit model is developed to extract polarization resistance from electrochemical impedance spectroscopy (EIS) data, which is integrated with stack voltage to construct a physically interpretable hybrid HI. Empirical mode decomposition (EMD) decomposes the hybrid HI into multi-

https://doi.org/10.53941/aiet.2026.100011

scale degradation components, while the Sparrow Search Algorithm (SSA) optimizes BiLSTM hyperparameters to improve prediction accuracy and robustness.The proposed fusion ahead prediction method (FAPM) is validated on more than 1000 h of real PEMFC durability data. Using only 182 h of FC2 data, FAPM achieves RMSE values of 0.008 and 0.0104 for 6-step and 10-step predictions, respectively, outperforming conventional data-driven methods in long-term degradation prediction.

Author Contributions

Conceptualization, H.L. and S.W.; methodology, H.L.; software, H.L. and D.Z.; validation, H.L., S.Y. and D.Z.; formal analysis, H.L.; investigation, H.L., S.Y. and L.Z.; data curation, H.L. and S.Y.; visualization, H.L. and D.Z.; supervision, S.W. and Q.C.; project administration, S.W.; writing, original draft preparation, H.L.; writing, review and editing, H.L., S.W. and Q.C. All authors have read and agreed to the published version of the manuscript.

Funding

This work was supported by the Youth Talent Project of the Scientific Research Program of Hubei Provincial Department of Education (Q20257501) and the 2026 University-Level Research Project of Wuhan Institute of Shipbuilding Technology (2026z06).

Institutional Review Board Statement

Not applicable.

Informed Consent Statement

Not applicable.

Data Availability Statement

The data that support the findings of this study are available from the corresponding author upon reasonable request.

Conflicts of Interest

The authors declare no conflict of interest.

Use of AI and AI-Assisted Technologies

No AI or AI-assisted technologies were used in the writing, analysis, or preparation of this manuscript.

References

1. Hu, Z.; Xu, L.; Li, J. A Reconstructed Fuel Cell Life-Prediction Model for a Fuel Cell Hybrid City Bus. *Energy Convers. Manag.* **2018**, *156*, 723–732.
2. Vichard, L.; Petrone, R.; Harel, F.; et al. Long Term Durability Test of Open-Cathode Fuel Cell System Under Actual Operating Conditions. *Energy* **2020**, *212*, 112813.
3. Li, Q.; Su, B.; Pu, Y.; et al. A State Machine Control Based on Equivalent Consumption Minimization for Fuel Cell/Supercapacitor Hybrid Tramway. *IEEE Trans. Transp. Electrif.* **2019**, *5*, 552–564.
4. Cuneo, A.; Zaccaria, V.; Tucker, D. Probabilistic Analysis of a Fuel Cell Degradation Model for Solid Oxide Fuel Cell and Gas Turbine Hybrid Systems. *Energy* **2017**, *141*, 2277–2287.
5. Olabi, A.G.; Wilberforce, T.; Abdelkareem, M.A. Fuel Cell Application in the Automotive Industry and Future Perspective. *Energy* **2021**, *214*, 118955.
6. Jouin, M.; Gouriveau, R.; Hissel, D.; et al. Prognostics of PEM Fuel Cell in a Particle Filtering Framework. *Int. J. Hydrogen Energy* **2014**, *39*, 481–494.
7. Jouin, M.; Gouriveau, R.; Hissel, D.; et al. PHM of Proton-Exchange Membrane Fuel Cells—A Review. *Chem. Eng. Trans.* **2013**, *33*, 1009.
8. Sutharssan, T.; Montalvao, D.; Chen, Y.K. A Review on Prognostics and Health Monitoring of Proton Exchange Membrane Fuel Cell. *Renew. Sustain. Energy Rev.* **2017**, *75*, 440–450.
9. Ou, M.; Zhang, R.; Shao, Z. A Novel Approach Based on Semi-Empirical Model for Degradation Prediction of Fuel Cells. *J. Power Sources* **2021**, *488*, 229435.
10. Farid, M. Data-Driven Method for Real-Time Prediction and Uncertainty Quantification of Fatigue Failure Under Stochastic Loading Using Artificial Neural Networks and Gaussian Process Regression. *Int. J. Fatigue* **2022**, *155*, 106415.

11. Ibrahim, M.; Steiner, N.Y.; Jemei, S.; et al. Wavelet-Based Approach for Online Fuel Cell Remaining Useful Lifetime Prediction. *IEEE Trans. Ind. Electron.* **2016**, *63*, 5057–5068.
12. Chen, K.; Laghrouche, S.; Djerdir, A. Degradation Model of Proton Exchange Membrane Fuel Cell Based on a Novel Hybrid Method. *Appl. Energy* **2019**, *252*, 113439.
13. Chen, K.; Laghrouche, S.; Djerdir, A. Prognosis of Fuel Cell Degradation Under Different Applications Using Wavelet Analysis and Nonlinear Autoregressive Exogenous Neural Network. *Renew. Energy* **2021**, *179*, 802–814.
14. Ma, J.; Liu, X.; Zou, X.; et al. Degradation Prognosis for Proton Exchange Membrane Fuel Cell Based on Hybrid Transfer Learning and Intercell Differences. *ISA Trans.* **2021**, *113*, 149–165.
15. Vichard, L.; Harel, F.; Ravey, A.; et al. Degradation Prediction of PEM Fuel Cell Based on Artificial Intelligence. *Int. J. Hydrog. Energy* **2020**, *45*, 14953–14963.
16. Zuo, J.; Lv, H.; Zhou, D.; et al. Deep Learning Based Prognostic Framework Towards Proton Exchange Membrane Fuel Cell for Automotive Application. *Appl. Energy* **2021**, *281*, 115937.
17. Wang, F.K.; Mamo, T.; Cheng, X.B. Bi-Directional Long Short-Term Memory Recurrent Neural Network with Attention for Stack Voltage Degradation from Proton Exchange Membrane Fuel Cells. *J. Power Sources* **2020**, *461*, 228170.
18. Ma, R.; Li, Z.; Breaz, E.; et al. Data-Fusion Prognostics of Proton Exchange Membrane Fuel Cell Degradation. *IEEE Trans. Ind. Appl.* **2019**, *55*, 4321–4331.
19. Hua, Z.; Zheng, Z.; Péra, M.C. Remaining Useful Life Prediction of PEMFC Systems Based on the Multi-Input Echo State Network. *Appl. Energy* **2020**, *265*, 114791.
20. Deng, Z.; Chan, S.H.; Chen, Q. Efficient Degradation Prediction of PEMFCs Using ELM-AE Based on Fuzzy Extension Broad Learning System. *Appl. Energy* **2023**, *331*, 120385.
21. Gouriveau, R.; Hilairet, M.; Hissel, D.; et al. IEEE PHM 2014 Data Challenge: Outline, Experiments, Scoring of Results, Winners. IEEE 2014 PHM Challenge, Technical Report, 2014. Available online: https://dx.doi.org/10.25666/DATAUBFC-2021-07-19 (accessed on 27 April 2026).
22. Tian, Z.; Wang, J.; Al-Durra, A. A Novel Aging Prediction Method of Fuel Cell Based on Empirical Mode Decomposition and Complexity Threshold Quantitative Criterion. *J. Power Sources* **2023**, *574*, 233120.
23. Lebreton, C.; Benne, M.; Damour, C.; et al. Fault Tolerant Control Strategy Applied to PEMFC Water Management. *Int. J. Hydrogen Energy* **2015**, *40*, 10636–10646.
24. Jia, C.; Zhou, J.; He, H. A Novel Energy Management Strategy for Hybrid Electric Bus with Fuel Cell Health and Battery Thermal- and Health-Constrained Awareness. *Energy* **2023**, *271*, 127105.
25. Li, Q.; Cai, L.; Yin, L.; et al. An Energy Management Strategy Considering the Economy and Lifetime of Multi-Stack Fuel Cell Hybrid System. *IEEE Trans. Transp. Electrif.* **2023**, *9*, 3498–3507.
26. Peng, F.; Zhao, Y.; Li, X.; et al. Development of Master-Slave Energy Management Strategy Based on Fuzzy Logic Hysteresis State Machine and Differential Power Processing Compensation for a PEMFC-LIB-SC Hybrid Tramway. *Appl. Energy* **2017**, *206*, 346–363.
27. Fletcher, T.; Thring, R.; Watkinson, M. An Energy Management Strategy to Concurrently Optimise Fuel Consumption & PEM Fuel Cell Lifetime in a Hybrid Vehicle. *Int. J. Hydrogen Energy* **2016**, *41*, 21503–21515.
28. Yang, Y.; Xu, Y. Degradation Prediction of Proton Exchange Membrane Fuel Cells with Model Uncertainty Quantification. *Renew. Energy* **2023**, *219*, 119525.